International Journal of Environmental Sciences
ISSN: 2229-7359
Vol. 11 No. 22s, 2025
https://www.theaspd.com/ijes.php

Combined Convection Heat Transfer In A Trapezoidal Enclosure With A Revolving Inner Cylinder For $H_2O - Cu - Al_2O_3$ Hybrid Nanofluid

Hajer Mohammed Hassan[1], Akeel Abdullah Mohammed[2],
[1] Al-Nahrain University, College of Engineering, Mech. Eng. Dept, hajhaj1999@gmail.com
[2]Al-Nahrain University, College of Engineering, Mech. Eng. Dept, akeel.a.mohammed@nahrainuniv@edu.iq

Abstract
A numerical analysis was executed using the Ansys program (ANSYS Fluent 2021 R2) to examine combined convection throughout a trapezoidal enclosure including a rotating cylinder as a source of heat. In this work, two different fluids were used: water and a hybrid nanofluid comprising water and Water − Cu − Al_2O_3. Along with the angled walls being insulated, the top and lower walls remain cold and stationary. Validation and comparison of the current study with earlier published studies have disclosed a substantial degree of agreement, with a mean relative disparity of about 1.9%. The results include a total of four internal cylinder places (center, right, top, and bottom), four tilted angles (0°, 45°, 90°, and 180°), and three different Richardson numbers (0.01, 1, and 10). The radius ratios are (0.20, 0.25). It is shown that the ideal location exhibiting the highest average Nusselt value throughout each angle (φ = 0°, 45°, and 90°) is at the bottom (0, −0.12). The greatest rate of Heat transmission happens when the angle is (φ = 180°) and the location is at the top (0, 0.12).

Keywords*: mixed convection, trapezoidal cavity, heat transfer, rotating cylinder, hybrid nanofluid.*

1. INTRODUCTION

In cavities, combined convection heat transmission may occur once the inner cylinder is moving actively. Researchers have placed a lot of emphasis on cavities with a moving cylinder because of its critical significance in industrial applications, where they have assessed the impact of diverse geometries, boundary conditions, and optimization techniques on heat transmission. Solar energy, thermal energy storage devices, and nuclear reactors are examples of industrial uses for this technology [1-4]. To improve heat transfer, mixed convection within cavities with one or more moving cylinders has been investigated using various techniques. Effective strategies include employing porous media [5–14], nanofluids, and hybrid nanofluids [15–29] to increase the base fluid's thermal conductivity. In addition, other techniques such as introducing multiple cylinders with different arrangements and orientations or applying a magnetic field inside the enclosure, along with many other optimization methods, have been proposed [30-44]. This work uses Ansys Fluent 2022 R1 software to do computational simulations of combined convection inside an angled trapezoidal recess, loaded by a hybrid nanofluid ($H_2O - Cu - Al_2O_3$) and containing a moving inner cylinder. The temperature of this cylinder, which serves as a heat source, is kept constant at T_h. On the other hand, the sloped surfaces are insulated with adiabatic techniques, and the stationary top and bottom are both cooled to the same temperature T_c. It is important to note that the cavity's walls are fully permanent. Several Richardson numbers were examined in this research: Ri = 0.01, 1, 10. Four locations for the inner cylinder (center, bottom, top, and right) and two radius ratio values (0.20 and 0.25) were also selected. Furthermore, four volume ratios of the hybrid nanoparticles (ϕ = 0\%, 4%, 6%, and 8%) and four distinct tilt angles (0°, 45°, 90°, and 180°) were examined.

International Journal of Environmental Sciences
ISSN: 2229-7359
Vol. 11 No. 22s, 2025
https://www.theaspd.com/ijes.php

2. The theoretical structure

2.1. Geometry Design and Assumptions

Using a 2D, stable, laminar combined convective flow, the thermal transmission inside a trapezoidal enclosure is numerically analyzed. It is presumed that the fluid medium behaves Newtonianly and is incompressible. By connecting the temperature and flow fields, the density change brought on by temperature variations is described using Boussinesq approximations. Internal heat production and the dissipative effects caused by viscosity are not included in this approach. The physical domain of the trapezoidal cavity system under study is schematically represented in Figure 1. The enclosure's sloped surfaces are separated by adiabatic techniques, and its two cold parallel surfaces are maintained at a steady temperature T_c in a stationary condition. At a temperature T_h, the revolving inner cylinder undergoes isothermal heating. To analyze the impact of the two radius ratios, this study analyzes two distinct inner cylinder radius (r_o) values. A counterflow is created when the shear flow from the internal cylinder motion is opposed by the free convection flow based on the temperature gradient in the enclosure due to the cavity's angle of inclination φ with respect to the x-axis.

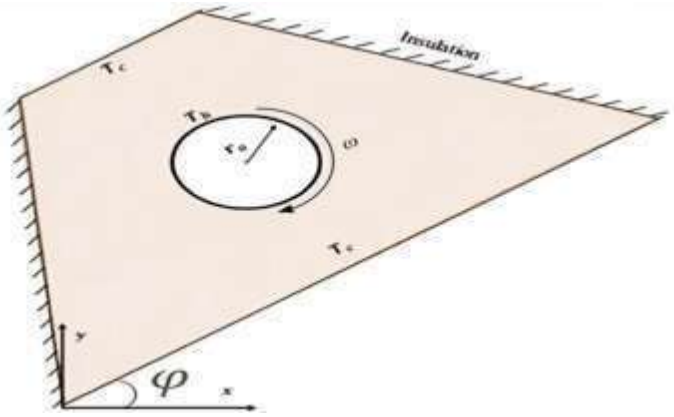

Figure 1. Basic Geometry.

2.2. Mathematical Equations and Formulation

The mass, momentum, and energy conservation equations in their dimensionless version are [45]:

$$\frac{\partial U}{\partial X}+\frac{\partial V}{\partial Y}=0 \tag{1}$$

$$U\frac{\partial U}{\partial X}+V\frac{\partial U}{\partial Y}=-\frac{\partial P}{\partial X}+Pr_{bf}\frac{\rho_{bf}\mu_{hnf}}{\rho_{hnf}\mu_{bf}}\left(\frac{\partial^2 U}{\partial X^2}+\frac{\partial^2 U}{\partial Y^2}\right) \tag{2}$$

$$U\frac{\partial V}{\partial X}+V\frac{\partial V}{\partial Y}=-\frac{\partial P}{\partial X}+Pr_{bf}\frac{\rho_{bf}\mu_{hnf}}{\rho_{hnf}\mu_{bf}}\left(\frac{\partial^2 V}{\partial X^2}+\frac{\partial^2 V}{\partial Y^2}\right)+4Ri\Omega^2R^4\times\frac{\rho_{bf}}{\rho_{hnf}}\left[1-\emptyset+\emptyset\frac{\rho_p\beta_p}{\rho_{bf}\beta_{bf}}\right]\theta \tag{3}$$

$$U\frac{\partial\theta}{\partial X}+V\frac{\partial\theta}{\partial Y}=\frac{k_{hnf}(\rho Cp)_{bf}}{k_{bf}(\rho Cp)_{hnf}}\left(\frac{\partial^2\theta}{\partial X^2}+\frac{\partial^2\theta}{\partial Y^2}\right) \tag{4}$$

The dimensionless variables may be expressed in the following way:

$$U=\frac{uL}{\alpha},\quad V=\frac{vL}{\alpha},\quad X=\frac{x}{L},\quad Y=\frac{y}{L},\quad \theta=\frac{T-T_c}{T_h-T_c},\qquad \nu=\frac{\mu}{\rho} \tag{5}$$

$$\alpha=\frac{k}{\rho Cp},\quad Pr_f=\frac{\nu_f}{\alpha_f},\quad \Omega=\frac{\omega L^2}{\alpha},\quad Ri=\frac{Ra\times Pr}{4\Omega^2R^4} \tag{6}$$

International Journal of Environmental Sciences
ISSN: 2229-7359
Vol. 11 No. 22s, 2025
https://www.theaspd.com/ijes.php

Table 1. It delineates the boundary conditions in a dimensionless format. The sign 'n' denotes the perpendicular alignment to the inclined surfaces.

	U	V	Θ
Top surface	0	0	0
Bottom surface	0	0	0
Left and right surfaces:	0	0	$\frac{\partial \theta}{\partial n} = 0$
Inner cylinder surface	ω * r	0	1

2.3. The fluid medium's physical and thermal properties

Computationally efficient equations for equivalent thermal properties were developed and demonstrated in [46–48]:

$$\rho_{hnf} = (1 - \varphi_{Cu} - \varphi_{Al_2O_3})\rho_f + \varphi_{Cu}\rho_{Cu} + \varphi_{Al_2O_3}\rho_{Al_2O_3} \quad (7)$$

$$(\rho\beta)_{hnf} = (1 - \varphi_{Cu} - \varphi_{Al_2O_3})(\rho\beta)_f + \varphi_{Cu}(\rho\beta)_{Cu} + \varphi_{Al_2O_3}(\rho\beta)_{Al_2O_3} \quad (8)$$

$$(\rho C_p)_{hnf} = (1 - \varphi_{Cu} - \varphi_{Al_2O_3})(\rho C_p)_f + \varphi_{Cu}(\rho C_p)_{Cu} + \varphi_{Al_2O_3}(\rho C_p)_{Al_2O_3} \quad (9)$$

$$\frac{k_{hnf}}{k_f} = \frac{\frac{\varphi_{Al_2O_3}k_{Al_2O_3} + \varphi_{Cu}k_{Cu}}{\varphi} + 2k_f + 2(\varphi_{Al_2O_3}k_{Al_2O_3} + \varphi_{Cu}k_{Cu}) - 2\varphi k_f}{\frac{\varphi_{Al_2O_3}k_{Al_2O_3} + \varphi_{Cu}k_{Cu}}{\varphi} + 2k_f - (\varphi_{Al_2O_3}k_{Al_2O_3} + \varphi_{Cu}k_{Cu}) + \varphi k_f} \quad (10)$$

$$\mu_{hnf} = \mu_f \frac{1}{(1-\varphi)^{2.5}} \quad (11)$$

Table 2. Properties of H_2O, Cu, Al_2O_3, and H_2O-Cu-Al_2O_3 hybrid nanofluid in terms of thermal and physical [12].

Material	Cp $(J/kg.K)$	ρ (kg/m^3)	k $(W/m.K)$	β $(1/K)$	$\mu(Pa.s)$
$H2O$	4179	997.1	0.613	21×10^{-5}	0.001003
Cu	385	8933	441	1.67×10^{-5}	-
$Al2O3$	765	3970	40	0.85×10^{-5}	-
H_2O – Cu - Al_2O_3 ($\Phi_{Cu} = 2\%$, $\Phi_{Al2O3} = 2\%$)	3399	1218	1.1239	3.7×10^{-4}	0.001110767

H2O – Cu - Al2O3 ($\Phi_{Cu} = 3\%$, $\Phi_{Al2O3} = 3\%$)	2854	1438	1.2586	3.1×10^{-4}	0.001235468
H2O – Cu - Al2O3 ($\Phi_{Cu} = 4\%$, $\Phi_{Al2O3} = 4\%$)	2454	1657	1.4053	2.6×10^{-4}	0.001380684

2.4. Grid Generation

The energy, momentum, and continuity equations for complicated geometries may be solved in two dimensions through the use of computational meshes. Structured and unstructured meshes are the two primary categories into which volumetric meshes fall. These mathematical formulas are converted into a curved coordinate system that is connected to the surface in structured meshes. Structured meshes are only a good choice for simple forms, though, because their creation necessitates a lot of work and frequent changes to the model design. Because of its extreme inefficiency when dealing with complicated geometries, this technique was not included in our study. On the other hand, unstructured meshes are used in this study since they are more suited for complicated geometries. Figure 2 illustrates the usage of a non-uniform, triangular, unstructured partition mesh.

2.5. Mesh Independence

To find the ideal number of mesh elements and their surface sizes for this specific shape, a mesh independence test was conducted. A Reynolds number of 100, a radius ratio of 0.25, and element sizes ranging from 1 to 0.8, 0.6, 0.4, and 0.3 were all included in the study. The mesh was unstructured, triangular, and non-uniform. The average Nusselt number's variation with element size is seen in Figure 3. The Nusselt number gave convergent findings at element size 0.3. As a result, a mesh with 43,660 pieces was chosen for this investigation as it provides a suitable balance between computing efficiency and accurate.

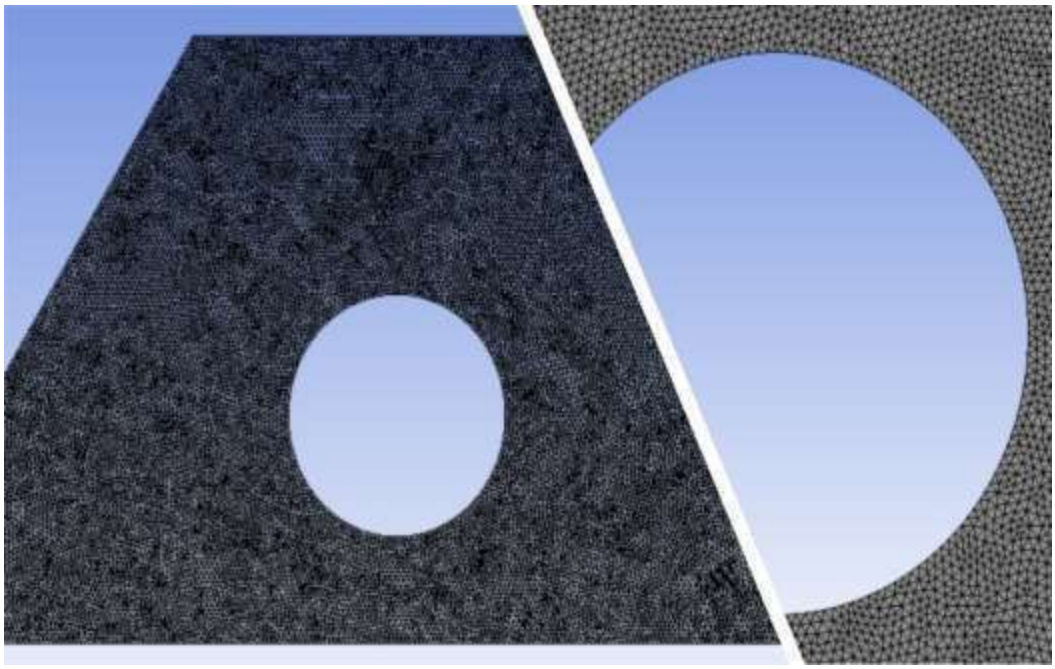

Figure 2. Mesh Generation

International Journal of Environmental Sciences
ISSN: 2229-7359
Vol. 11 No. 22s, 2025
https://www.theaspd.com/ijes.php

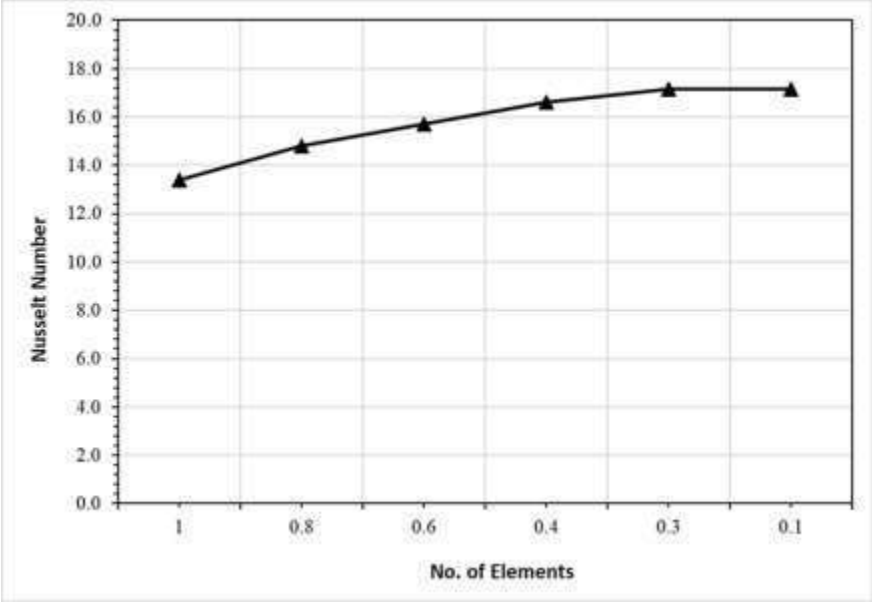

.
Figure 3. Convergence of the mean Nusselt numbers and element size.

2.6. The Computational Method

Numerous aspects of the computation strategy are impacted by the solution approaches. ANSYS Fluent 2022 R1 software was used in this work to resolve the mathematical equations in accordance with the given boundary conditions. Mesh creation is the first step in the procedure, after which the program uses the SIMPLE algorithm to solve the mathematical problems one after the other. Furthermore, momentum, pressure, turbulent kinetic energy, and turbulence dissipation rate in the upwind direction were all subjected to a second-order spatial discretization. The local Nu of the spinning cylinder is provided in this study using the SIMPLE approach, which is frequently utilized for resolving the Navier-Stokes equations:

$$Nu_{ave} = \frac{1}{A}\int_0^A \frac{-k_{nf,0}}{k_f}\frac{\partial\theta}{\partial X}|_{X=0}\, dY \qquad (3.13)$$

The average Nusselt number (Nu) for the heated cylindrical rotating surface is represented by:

$$Nu_{ave} = \frac{1}{L}\int_0^L Nu_x\, dx \qquad (3.12)$$

3. Code Validation

By contrasting the current simulation method with the flow and heat transmission findings disclosed by Khanafer et al. [49], the correctness of the method was confirmed. A comparative analysis of the average Nusselt number values collected in the two experiments is presented in Table 3. A square container with a chilly upper surface advancing towards the positive x direction and a hot, stationary lower wall was the subject of this study's examination of mixed convective air flow. A circular spinning inner cylinder with RR = 0.2 is within the container. To validate the results, four values of the Richardson number were selected, and air was utilized as the medium with a Prandtl number of 0.7. The comparison revealed that, with a 1.9% relative difference, the mean Nusselt numbers from the two simulations were quite similar.

International Journal of Environmental Sciences
ISSN: 2229-7359
Vol. 11 No. 22s, 2025
https://www.theaspd.com/ijes.php

Table 3. Validation of average Nusselt number values for the present project against the study of Khanafer et al. [49].

Ri	$Nu_{previous}$[26]	$Nu_{current}$	$difference$
0.01	4.28	4.37	2.1%
1	4.40	4.51	2.5%
5	4.77	4.85	1.6%
10	4.99	5.06	1.4%

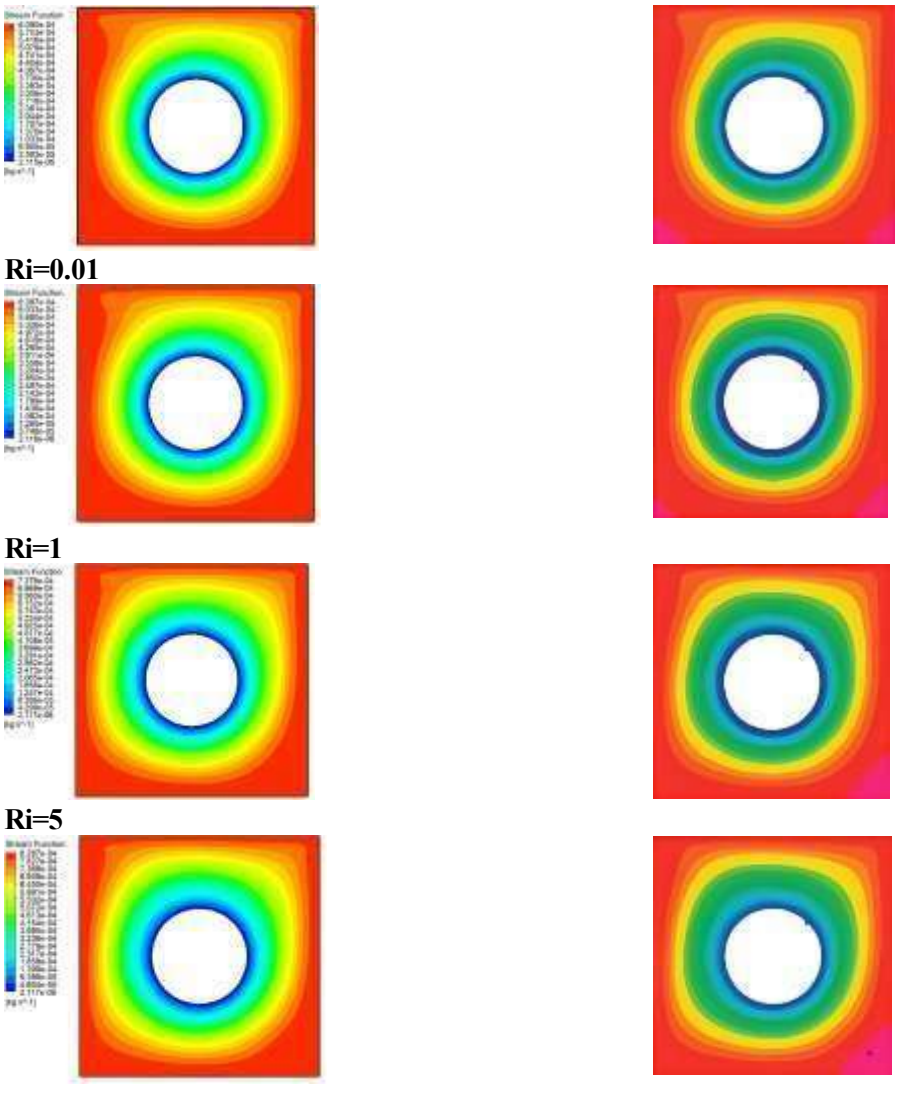

Figure 4. Streamlines maps for the current simulation approach (left) and the study of Khanafer

et al. [49] (right).

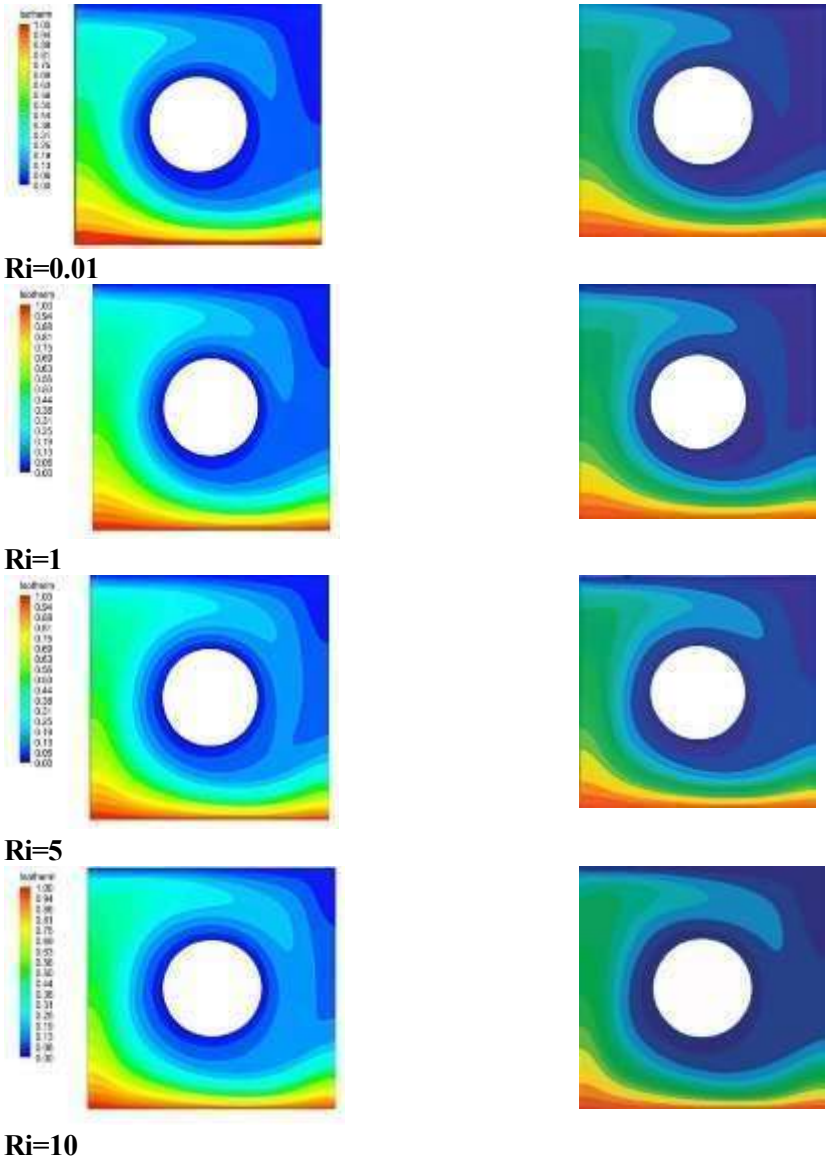

Figure 5. Isotherm maps for the current simulation methodology (left) and the study of Khanafer et al. [49] (right).

4. RESULTS AND DISCUSSION

4.1 Streamline Maps and Isotherm Maps

The implications concerning the Richardson numbers affect the flow with isothermal lines within an enclosure with a rotating cylinder and an 8% hybrid nanoparticle volume fraction at several degrees of inclination (φ=0°, 45°, 90°, and 180°) are shown in Figure 6. The behavior of flow lines and isothermal lines is greatly influenced by volume fractions, degrees of inclination, and Richardson numbers. The

Richardson number, $Ri=Gr/Re^2$, indicates how significant free convection is in comparison to forced convection.

Figure 6 demonstrates that a Richardson number of 0.01 exerts negligible influence on the streamline profile at all degrees of enclosure inclination due to the overwhelming effect of the main flow. The visibility of vortices may be diminished owing to the prevalence of forced convection. The vortices may seem to intensify as Ri exceeds 1 and 10 due to the augmented Impacts of the second flow resulting from vigorous free convection. The fluid generally flows in a similar orientation to the spinning cylinder. Upon contact with the nearest wall, the fluid's velocity is altered to the opposing orientation, forming a vortex or rotational movements.

When the Richardson number is 0.01, the substantial flow generated by the cylinder's rotating movement causes the principal flow patterns to occupy the entire hollow. The shear influences induced by the cylinder's motion are evident at all incline angles. Thus, the isotherms exhibited inadequate growth inside the thermo-hydrodynamic boundary layers. As a result, the temperature fluctuations inside the confined area are negligible. When the Richardson number escalates, the temperature gets higher, causing the isotherms to migrate out of the hot cylinder toward the cooler sides. As the Richardson number increases, the thermal plume intensifies. The direction is predominantly influenced by the fluid type (with or without a hybrid nanoparticle), the Richardson number, and the tilt. An increase in the Richardson number to the 1 signifies the occurrence of mixed convection. In this instance, two currents exist: the supportive current and the adversarial one. As the primary flow path coincides considering the orientation of the buoyancy force (downwards), the flow is classified as supporting. Whenever the orientation of the inertial force (primary stream) is ascendant, the stream is classified as opposed. Also, the flow pattern contributes to the present investigation.

Figure 6 shows the primary vortex spreads around the cylinder at a Richardson number of 1 when the slope is 90°. This suggests that the maximum flow function is weaker, considering the state of the dominant forceful convection with a 0.01 Richardson number. As the main flow increases, the vortex strength rises (by enhancing the velocity produced by the movable wall and decreasing Ri to 0.01), regardless of incorporating hybrid nanoparticles integrated with the initial liquid. The vortex divides to form two potent portions in conditions of predominant free convection (Richardson number equals 10). Consequently, vigorous free convection flows.

At a slope degree of about 45°, the configuration of the streamlines nearly mimics that of a 90° inclined slope. The principal vortex bifurcates to form two diminished segments with a Richardson number of 1. Nevertheless, the vortex retains its potency while the Richardson number equals 10, attributable to the preeminent influence of natural convection. At a Richardson number equal to 0.01, the vortex exhibits a greater intensity compared with a Richardson number equal to 1; however, it has diminished intensity compared to a Richardson number equal to 10. Integrating hybrid nanoparticles into an initial fluid with a substantial volume percent, with a Richardson number equal to 10, produces significant and minor vortices. The streamlines inside a hollow, involving a bottom-spinning cylinder having a radius ratio value of 0.2 and A tilt of 180°, are apparent. The major vortex is often still focused around the cylinder with a Richardson number equal to 0.01, owing to heightened shearing operation during this region caused by predominant forced convection. The vortex enlarges and expands via integrating a hybrid nanoparticle with a volumetric fraction equal to 8 percent, owing to the substantial impact of the primary stream generated by the cylinder's motion. As the Richardson number approaches 1, the main vortex will remain localized around the cylinder; however, it will progressively fragment into vortices of differing densities owing to the interplay between forced flow and natural thermal processes. The behaviour in enclosed enclosures contrasts with the behaviour in open conduits, while the primary flow is diminished to the benefit of the second flow. A couple of

significant vortices can be seen on either side inside the enclosure. In comparison to different Richardson numbers, that is anticipated to exhibit a heightened rate of transmission of heat.

With a Richardson number equal to 10, the influences of natural convection supersede forced convection. Buoyancy amplifies primary flow, reinforcing convection when the Richardson number gets higher. Consequently, the isothermal lines get more pronounced towards the cool surface. The evolution of the thermo-hydrodynamic boundary layer will transpire alongside the thermally contrasting surfaces. Moreover, the maximum temperature diminishes, leading to an elevated thermal transmission rate. Furthermore, in the surrounding area of the high-temperature cylinder surface, it is evident that the isotherm generates more pronounced temperature gradients. The isotherms encircle the heated cylinder, although their intensity diminishes near the cylinder owing to the prevailing influence of free convection. In this scenario, the isotherms shift away from the heated surface towards the cooler walls, where increased heat transfer occurs, facilitated by the free convection that disperses heat from the cylinder. The thermal column or steep temperature gradient will be less intense than in instances of predominant forced convection, yet a subtler thermal gradient may manifest, extending further from the cylinder. Elevating the volume percentage of hybrid nanoparticles over 10% is often anticipated to diminish the thermal diffusivity of the liquid and adversely influence the flow dynamics and thermal transfer within the hollow.

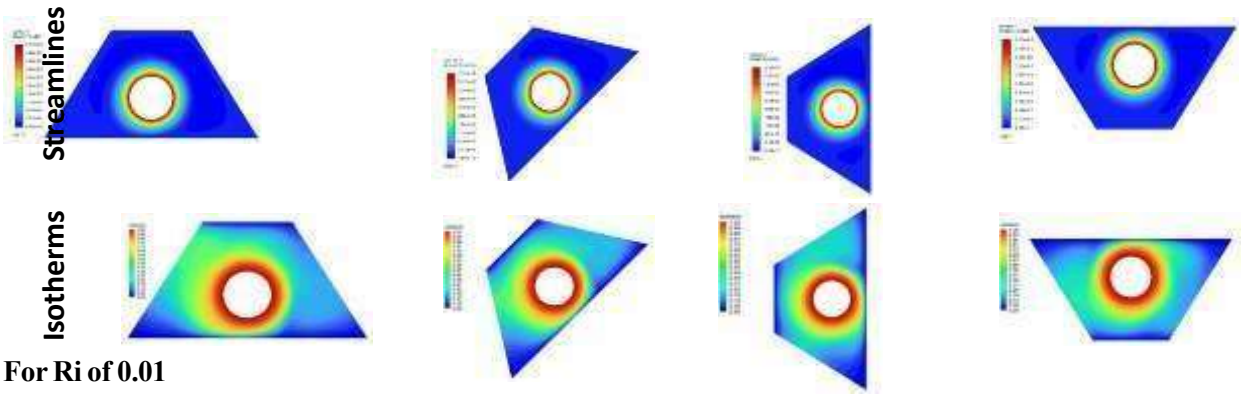

For Ri of 0.01

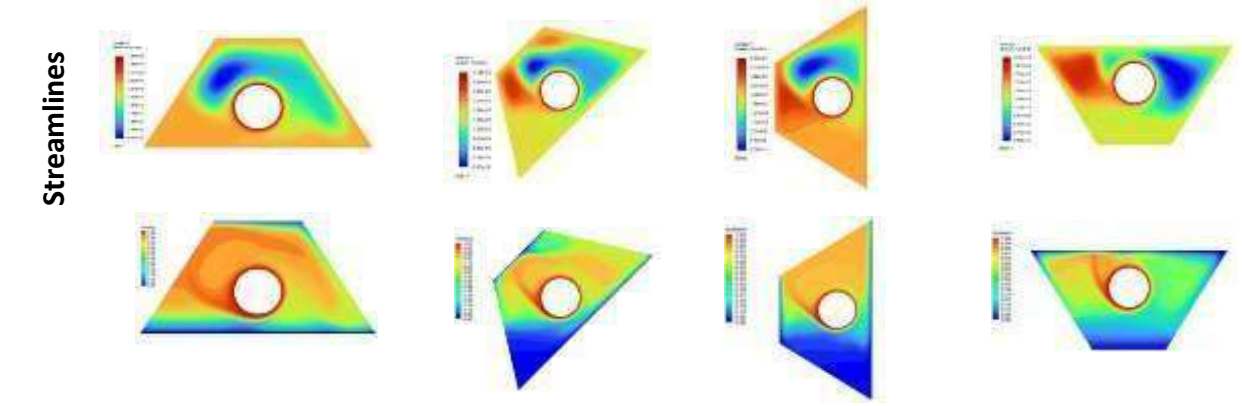

For Ri of 1

International Journal of Environmental Sciences
ISSN: 2229-7359
Vol. 11 No. 22s, 2025
https://www.theaspd.com/ijes.php

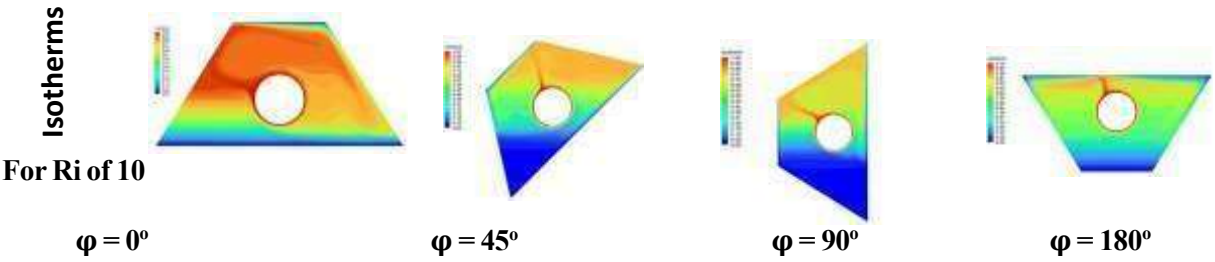

Figure 6. Optimise, streamline, and isotherm maps inside an enclosure, including a spinning cylinder on the base location with RR = 0.2 and ϕ = 0.08.

4.2 The Mean Nusselt Number

Figure 7 depicts the average Nusselt number as an indication of the volumetric percent of hybrid nanoparticles across several Richardson numbers and enclosure angles of tilt (φ=0°, 45°, 90°, and 180°). An elevation in the Richardson number has been seen to correlate with an increase in the mean Nusselt number across all volume fractions. For Ri=10 and hybrid nanoparticle concentration percentages of φ = 0, 0.04, and 0.06, the mean Nusselt numbers at φ = 90° exceed those at other inclined angles. Furthermore, in comparison to other inclination angles, the angle φ = 90° has the highest average Nusselt number for ϕ = 0.08. The findings suggest that an augmentation in the volumetric percent of hybrid nanoparticles improves the rate of heat (the mean Nusselt number) owing to the enhanced thermal conductivity of the working fluid.

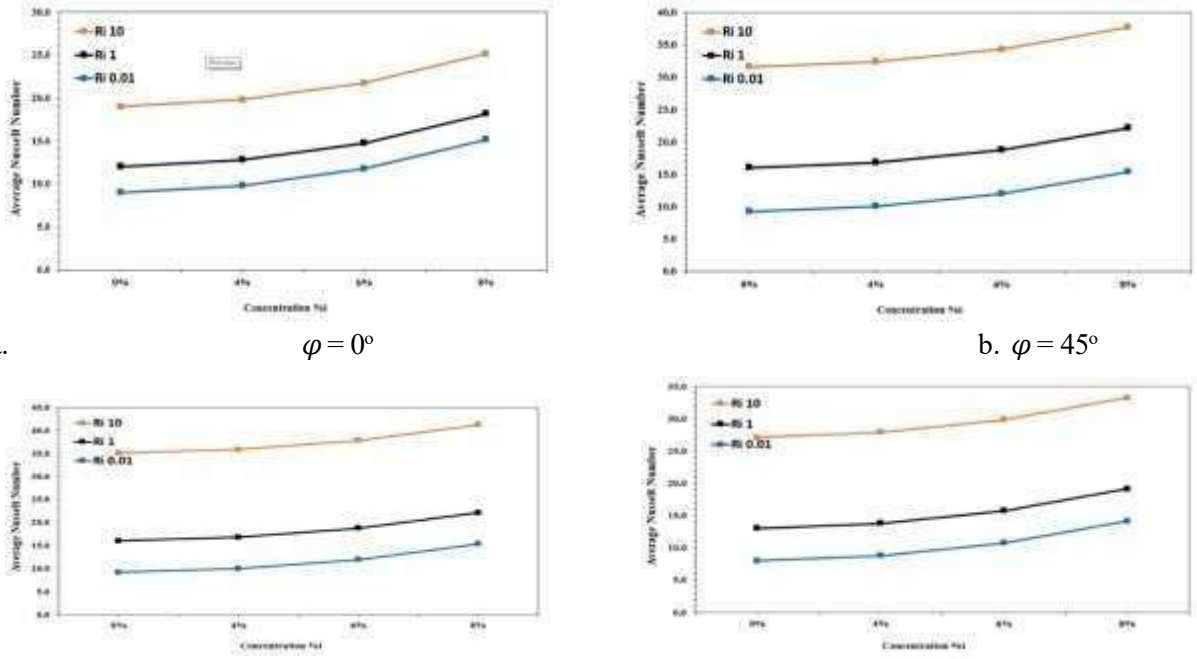

a. φ = 0° b. φ = 45°

c. φ = 90° d. φ = 180°

Figure 7. The average Nusselt number around the internal cylinder for various hybrid nanoparticle volume fractions and slopes of tilt.

4.3 Friction Losses

Figure 8 illustrates the losses in pressure, reflecting the loss of friction as an indicator of the volumetric percent

of hybrid nanoparticles across several Richardson numbers and enclosure tilt of (φ = 0°, 45°, 90°, 180°). The pressure drops experience a little increase for Ri values of 0.01 and 1, but a substantial escalation occurs for a Ri value of 10 as the volume% % of hybrid nanoparticles grows. This results from the heightened viscosity caused by the incorporation of hybrid nanoparticles, which causes elevated shear stress as well as loss of friction. The pressure loss escalates based on the Richardson number for φ = 0°, 45°, 90°, and 180°, as seen in the figure. The pressure drops figures for Ri = 0.01 and 1 are virtually indistinguishable in these cases. They exemplify the most effective cases of surmounting high-pressure variations.

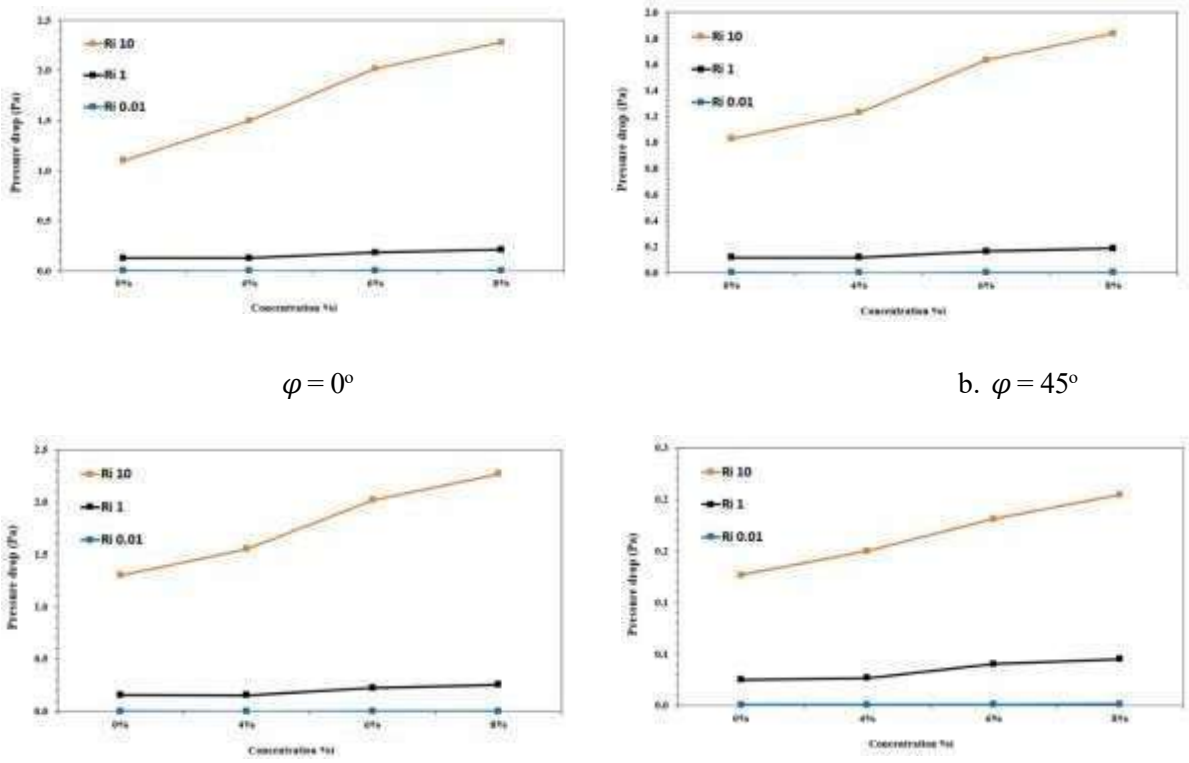

a. $\varphi = 0^o$ b. $\varphi = 45^o$

c. $\varphi = 90^o$ d. $\varphi = 180^o$

Figure 8. The losses in pressure within the enclosure for various hybrid nanoparticles fractions of volume and slope angles.

5. CONCLUSIONS

1. The rate of transferring heat increases alongside an increase in the Richardson number, attributed to the enhancement from free convection currents.
2. As the volume percent of hybrid nanoparticles increases, the heat transmission mechanism is typically enhanced.
3. At inclined angles of 45° and 90°, the increase in streamlines is much larger at Ri=1 and Ri=10 compared to when the Richardson number is 0.01.
4. A Richardson number equals 10 across each angle of inclination, and the hybrid nanoparticle volume percent yields the greatest value of maximum stream function.

5. In closed enclosures, lowering the main flow to the detriment of the second one results in behaviors that are different from those seen in an open conduit.
6. As Ri increases from 0.01 to 1, the thermal plume seems to revolve in a clockwise direction around the heating circular cylinder.
7. With a Richardson number equal to 10 with hybrid nanoparticles volumetric percents of 0%, 4%, 6%, and 8%, the mean Nusselt number for an inclined angle of 90° is higher than those for the other degrees of inclination.
8. At Ri=10, the pressure losses appeared to rise according to the Richardson numbers at inclined angles of 0°, 45°, 90°, and 180°.

Abbreviations:

Al_2O_3 = Aluminum Oxide

H_2O = Water

Cu = Copper

CFD = Computational Fluid Dynamics

Gr = Grashof Number ($\frac{g\beta L^3(T_h - T_c)}{P^2}$)

f

h = Convective Heat Transfer Coefficient (W/m^2K)

C_p = Specific Heat ($J/kg.K$)

k = Thermal Conductivity ($W/m.K$)

g = Gravitational Acceleration (m/s^2)

Nu = Nusselt Number

Pr = Prandtl Number ($\frac{Pf}{\alpha f}$)

Re = Reynolds Number ($\frac{U_o L}{Pf}$)

Ri = Richardson Number ($\frac{Gr}{Re^2}$)

RR = Radius Ratio

u = Velocity in x-axis (m/s)

U = Non-Dimensional Velocity in x-axis

U_o = Lid Velocity (m/s)

v = Velocity in y-axis (m/s)

V = Non-Dimensional Velocity in y-axis

T = Temperature (K)
] = Dimensionless Temperature
P = Dimensionless Pressure

x, y = Space Coordinates

X, Y = Dimensional Space Coordinates

Greek Symbols:

α = Thermal Diffusivity ($k/\rho C_p$)

ρ = Density (kg/m^3)
β = Coefficient of Thermal Expansion (CTE)
($1/k$)
μ = Absolute Viscosity ($Pa.\ s$)

ν = Kinematical Viscosity (m^2/s)
ϕ = Volume Percentage of Nanoparticles
φ = Angle of Inclination (°)
ω = Angular speed
Ω = Dimensionless angular speed

Subscripts:

f = Base Fluid

hnf = Hybrid Nanofluid
T_c = Cold Temperature
T_h = Hot Temperature

REFERENCES

1. Selimefendigil, F., Ismael, M. A., & Chamkha, A. J. (2017). Mixed convection in superposed nanofluid and porous layers in square enclosure with inner rotating cylinder. *International Journal of Mechanical Sciences*, *124*, 95-108. https://doi.org/10.1016/j.ijmecsci.2017.03.007.
2. Hussain, S. H., & Hussein, A. K. (2011). Mixed convection heat transfer in a differentially heated square enclosure with a conductive rotating circular cylinder at different vertical locations. *International Communications in Heat and Mass Transfer*, *38*(2), 263-274. https://doi.org/10.1016/j.icheatmasstransfer.2010.12.006.
3. Jasim, L. M., Hamzah, H., Canpolat, C., & Sahin, B. (2021). Mixed convection flow of hybrid nanofluid through a vented enclosure with an inner rotating cylinder. International Communications in Heat and Mass Transfer, 121, 105086. https://doi.org/10.1016/j.icheatmasstransfer.2020.105086.
4. Shirazi, M., Shateri, A., & Bayareh, M. (2018). Numerical investigation of mixed convection heat transfer of a nanofluid in a circular enclosure with a rotating inner cylinder. *Journal of Thermal Analysis and Calorimetry*, *133*, 1061-1073. https://doi.org/10.1007/s10973-018-7186-y.
5. Misirlioglu, A. (2006). The effect of rotating cylinder on the heat transfer in a square cavity filled with porous medium. *International journal of engineering science*, *44*(18-19), 1173-1187. https://doi.org/10.1016/j.ijengsci.2006.07.008.

6. Chamkha, A. J., Selimefendigil, F., & Ismael, M. A. (2016). Mixed convection in a partially layered porous cavity with an inner rotating cylinder. *Numerical Heat Transfer, Part A: Applications*, *69*(6), 659-675. https://doi.org/10.1080/10407782.2015.1081027.
7. Malla, L. K., Jena, S. K., Mahapatra, S. K., & Chamkha, A. J. (2018). Mixed convection inside a fluid-porous composite cavity with centrally rotating cylinder. *Heat Transfer—Asian Research*, *47*(4), 684-701. https://doi.org/10.1002/htj.21336.
8. Hussein, A. K., Hamzah, H. K., Ali, F. H., & Kolsi, L. (2020). Mixed convection in a trapezoidal enclosure filled with two layers of nanofluid and porous media with a rotating circular cylinder and a sinusoidal bottom wall. *Journal of Thermal Analysis and Calorimetry*, *141*, 2061-2079. https://doi.org/10.1007/s10973-019-08963-6.
9. Abdulsahib, A. D., & Al-Farhany, K. (2020, November). Numerical Investigation of the nanofluid mixed convection on two layers enclosure with rotating cylinder: High Darcy Number Effects. In *IOP Conference Series: Materials Science and Engineering* (Vol. 928, No. 2, p. 022001). IOP Publishing. https://doi.org/10.1088/1757-899X/928/2/022001.
10. Cicek, O., Baytaş, A. F., & Baytaş, A. C. (2021). Entropy generation of mixed convection of SWCNT–water nanofluid filled an annulus with a rotating cylinder and porous lining under LTNE. *International Journal of Numerical Methods for Heat & Fluid Flow*, *31*(5), 1588-1617. https://doi.org/10.1108/HFF-04-2020-0229.
11. Ali, F. H., Hamzah, H. K., Hussein, A. K., Jabbar, M. Y., & Talebizadehsardari, P. (2020). MHD mixed convection due to a rotating circular cylinder in a trapezoidal enclosure filled with a nanofluid saturated with a porous media. *International Journal of Mechanical Sciences*, *181*, 105688. https://doi.org/10.1016/j.ijmecsci.2020.105688.
12. Al-Farhany, K., & Abdulsahib, A. D. (2021). Study of mixed convection in two layers of saturated porous medium and nanofluid with rotating circular cylinder. *Progress in Nuclear Energy*, *135*, 103723. https://doi.org/10.1016/j.pnucene.2021.103723.
13. Abderrahmane, A., Qasem, N. A., Younis, O., Marzouki, R., Mourad, A., Shah, N. A., & Chung, J. D. (2022). MHD hybrid nanofluid mixed convection heat transfer and entropy generation in a 3-D triangular porous cavity with zigzag wall and rotating cylinder. *Mathematics*, *10*(5), 769. https://doi.org/10.3390/math10050769.
14. Maneengam, A., Bouzennada, T., Abderrahmane, A., Ghachem, K., Kolsi, L., Younis, O., ... & Weera, W. (2022). Numerical study of 3D MHD mixed convection and entropy generation in trapezoidal porous enclosure filled with a hybrid nanofluid: effect of zigzag wall and spinning inner cylinder. *Nanomaterials*, *12*(12), 1974. https://doi.org/10.3390/nano12121974.
15. Sheikhzadeh, G. A., Teimouri, H., & Mahmoodi, M. (2013). Numerical study of mixed convection of nanofluid in a concentric annulus with rotating inner cylinder. *Challenges in Nano and Micro Scale Science and Technology*, *1*(1), 26-36. https://doi.org/10.7508/tpnms.2013.01.003.
16. Selimefendigil, F., & Öztop, H. F. (2014). MHD mixed convection of nanofluid filled partially heated triangular enclosure with a rotating adiabatic cylinder. *Journal of the Taiwan Institute of Chemical Engineers*, *45*(5), 2150-2162. https://doi.org/10.1016/j.jtice.2014.06.018.
17. Wang, Y. F., Xu, X., Tian, T., Fan, L. W., Wang, W. L., & Yu, Z. T. (2015). Laminar mixed convection heat transfer of SiC-EG nanofluids in a triangular enclosure with a rotating inner cylinder: Simulations based on the measured thermal conductivity and viscosity. *J. Zhejiang Univ. Sci. A*, *16*(6), 478-490. https://doi.org/10.1631/jzus.A1400120.
18. Selimefendigil, F., & Öztop, H. F. (2015). Mixed convection in a two-sided elastic walled and SiO2 nanofluid filled cavity with internal heat generation: Effects of inner rotating cylinder and nanoparticle's shape. *Journal of Molecular Liquids*, *212*, 509-516. https://doi.org/10.1016/j.molliq.2015.09.037.
19. Selimefendigil, F., Öztop, H. F., & Abu-Hamdeh, N. (2016). Mixed convection due to rotating cylinder in an internally heated and flexible walled cavity filled with SiO2–water nanofluids: effect of nanoparticle shape. *International Communications in Heat and Mass Transfer*, *71*, 9-19. https://doi.org/10.1016/j.icheatmasstransfer.2015.12.007.
20. Alsabery, A. I., Ismael, M. A., Chamkha, A. J., & Hashim, I. (2018). Numerical investigation of mixed convection and entropy generation in a wavy-walled cavity filled with nanofluid and involving a rotating cylinder. *Entropy*, *20*(9), 664. https://doi.org/10.3390/e20090664.
21. Chamkha, A. J., & Selimefendigil, F. (2019). MHD mixed convection of nanofluid due to an inner rotating cylinder in a 3D enclosure with a phase change material. *International Journal of Numerical Methods for Heat & Fluid Flow*, *29*(10), 3559-3583. https://doi.org/10.1108/HFF-07-2018-0364.
22. Selimefendigil, F., Oztop, H. F., & Abu-Hamdeh, N. H. (2019). Mixed convection due to a rotating cylinder in a 3D corrugated cavity filled with single walled CNT-water nanofluid. *Journal of Thermal Analysis and Calorimetry*, *135*(1), 341-355. https://doi.org/10.1007/s10973-018-7068-3.
23. Selimefendigil, F., Oztop, H. F., & Chamkha, A. J. (2019). Analysis of mixed convection and entropy generation of nanofluid filled triangular enclosure with a flexible sidewall under the influence of a rotating cylinder. *Journal of Thermal Analysis and Calorimetry*, *135*, 911-923. https://doi.org/10.1007/s10973-018-7317-5,
24. Selimefendigil, F., & Öztop, H. F. (2019). Conjugate mixed convection of nanofluid in a cubic enclosure separated with a conductive plate and having an inner rotating cylinder. *International Journal of Heat and Mass Transfer*, *139*, 1000-1017. https://doi.org/10.1016/j.ijheatmasstransfer.2019.05.053.

25. Ahmed, S. Y., Jabbar, M. Y., Hamzah, H. K., Ali, F. H., & Hussein, A. K. (2020). Mixed convection of nanofluid in a square enclosure with a hot bottom wall and a conductive half-immersed rotating circular cylinder. *Heat Transfer*, *49*(8), 4173-4203. https://doi.org/10.1002/htj.21822.
26. Ali, M. M., Akhter, R., Alim, M. A., & Miah, M. M. (2022). Magnetic-Mixed Convection in Nanofluid-Filled Cavity Containing Baffles and Rotating Hollow-Cylinders with Roughness Components. *Mathematical Problems in Engineering*, *2022*(1), 3044930. https://doi.org/10.1155/2022/3044930.
27. Alsabery, A. I., Alshukri, M. J., Jabbar, N. A., Eidan, A. A., & Hashim, I. (2022). Entropy generation and mixed convection of a nanofluid in a 3D wave tank with rotating inner cylinder. *Energies*, *16*(1), 244. https://doi.org/10.3390/en16010244.
28. Cherif, B. M., Abderrahmane, A., Saeed, A. M., Qasem, N. A., Younis, O., Marzouki, R., ... & Shah, N. A. (2022). Hydrothermal and entropy investigation of nanofluid mixed convection in triangular cavity with wavy boundary heated from below and rotating cylinders. *Nanomaterials*, *12*(9), 1469. https://doi.org/10.3390/nano12091469.
29. Abood, F. A., Yaseen, S. J., Mohammed, I. G., Homod, R. Z., & Mohammed, H. I. (2024). Enhancing thermal performance in a magnetized square cavity: novel insights from mixed convection of Ag-MgO nanofluid around a rotating cylinder. *International Journal of Thermofluids*, *22*, 100630. https://doi.org/10.1016/j.ijft.2024.100630.
30. Rahman, M., Alim, M. A., Saha, S., & Chowdhury, M. K. (2008). Mixed convection in a vented square cavity with a heat conducting horizontal solid circular cylinder. *Journal of naval architecture and marine engineering*, *5*(2), 37-46. https://doi.org/10.3329/jname.v5i2.2504.
31. Selimefendigil, F., & Öztop, H. F. (2014). Estimation of the mixed convection heat transfer of a rotating cylinder in a vented cavity subjected to nanofluid by using generalized neural networks. *Numerical Heat Transfer, Part A: Applications*, *65*(2), 165-185. https://doi.org/10.1080/10407782.2013.826109.
32. Selimefendigil, F., & Chamkha, A. J. (2020). MHD mixed convection of nanofluid in a three-dimensional vented cavity with surface corrugation and inner rotating cylinder. *International Journal of Numerical Methods for Heat & Fluid Flow*, *30*(4), 1637-1660. https://doi.org/10.1108/HFF-10-2018-0566.
33. Priam, S. S., Saha, R., & Saha, S. (2021, February). Pure mixed convection inside a vented square cavity with an isothermally heated rotating cylinder. In *AIP Conference Proceedings* (Vol. 2324, No. 1). AIP Publishing. https://doi.org/10.1063/5.0037533.
34. Abderrahmane, A., Alqsair, U. F., Guedri, K., Jamshed, W., Nasir, N. A. A., Majdi, H. S., ... & Marzouki, R. (2022). Analysis of mixed convection of a power-law non-Newtonian nanofluid through a vented enclosure with rotating cylinder under magnetic field. *Annals of Nuclear Energy*, *178*, 109339. https://doi.org/10.1016/j.anucene.2022.109339.
35. Costa, V. A. F., & Raimundo, A. M. (2010). Steady mixed convection in a differentially heated square enclosure with an active rotating circular cylinder. *International Journal of Heat and Mass Transfer*, *53*(5-6), 1208-1219. https://doi.org/10.1016/j.ijheatmasstransfer.2009.10.007.
36. Khan, M., Khan, A. A., & Hasan, M. N. (2016, July). Numerical study of mixed convection heat transfer from a rotating cylinder inside a trapezoidal enclosure. In *AIP Conference Proceedings* (Vol. 1754, No. 1). AIP Publishing. https://doi.org/10.1063/1.4958427.
37. Nair, Y., Shakkottai, V., & Prasad, B. V. S. S. S. (2016, July). Mixed convection heat transfer in an annulus with rotating inner cylinder. In *Heat Transfer Summer Conference* (Vol. 50336, p. V002T15A004). American Society of Mechanical Engineers. https://doi.org/10.1115/HT2016-7148.
38. Alam, M., Kamruzzaman, K., Ahsan, F., & Hasan, M. N. (2016, July). Mixed convection heat transfer inside a differentially heated square enclosure in presence of a rotating heat conducting cylinder. In *AIP Conference Proceedings* (Vol. 1754, No. 1). AIP Publishing. https://doi.org/10.1063/1.4958426.
39. Selimefendigil, F., & Öztop, H. F. (2016). MHD mixed convection and entropy generation of power law fluids in a cavity with a partial heater under the effect of a rotating cylinder. *International Journal of Heat and Mass Transfer*, *98*, 40-51. https://doi.org/10.1016/j.ijheatmasstransfer.2016.02.092.
40. Alam, M., Kamruzzaman, K., Saha, S., & Hasan, M. N. (2017, June). Effect of location of a rotating circular cylinder and heat source on mixed convection heat transfer characteristics inside a square enclosure with discrete heater at the bottom wall. In *AIP Conference Proceedings* (Vol. 1851, No. 1). AIP Publishing. https://doi.org/10.1063/1.4984730.
41. Shahriar, M., & Mamun, M. A. H. (2019, July). Magnetic field effect on mixed convection in ferrofluid filled c-shaped cavity with rotating circular cylinder at different positions with intruded heated sides. In *AIP Conference Proceedings* (Vol. 2121, No. 1). AIP Publishing. https://doi.org/10.1063/1.5115920.
42. Selimefendigil, F., & Öztop, H. F. (2020). Mixed convection in a PCM filled cavity under the influence of a rotating cylinder. *Solar Energy*, *200*, 61-75. https://doi.org/10.1016/j.solener.2019.05.062.
43. Azim, E., Sagor, M. J. H., Hasan, A. B. M. R., & Saha, S. (2021, February). Investigation on conjugate mixed convection inside a square cavity with heat generating rotating circular cylinder. In *AIP Conference Proceedings* (Vol. 2324, No. 1). AIP Publishing. https://doi.org/10.1063/5.0037524.

44. Mohammed, A. (2021). Natural convection heat transfer inside horizontal circular enclosure with triangular cylinder at different angles of inclination. *Journal of Thermal Engineering*, *7*(1), 240-254. https://doi.org/10.18186/thermal.849812.
45. AI, F., & ZM, A. (2021). Mixed Convection of Heat Transfer around Rotating Cylinders inside Enclosure Filled with Nano Fluid. *International Research Journal of Innovations in Engineering and Technology,* 05(10), 51–64. https://doi.org/10.47001/irjiet/2021.510010.
46. Brinkman, H. C. (1952). The viscosity of concentrated suspensions and solutions. *The Journal of Chemical Physics,* 20(4), 571. https://doi.org/10.1063/1.1700493.
47. Alsabery, A. I., Hashim, I., Hajjar, A., Ghalambaz, M., Nadeem, S., & Pour, M. S. (2020). Entropy generation and natural convection flow of hybrid nanofluids in a partially divided wavy cavity including solid blocks. *Energies,* 13(11), 2942. https://doi.org/10.3390/en13112942.
48. El-Zahar, E. R., Rashad, A. M., Saad, W., & Seddek, L. F. (2020). Magneto-Hybrid Nanofluids Flow via Mixed Convection past a Radiative Circular Cylinder. *Scientific Reports,* 10(1). https://doi.org/10.1038/s41598-020-66918-6.
49. Khanafer, K., & Aithal, S. M. (2017). Mixed convection heat transfer in a lid-driven cavity with a rotating circular cylinder. *International Communications in Heat and Mass Transfer*, *86*, 131-142. https://doi.org/10.1016/j.icheatmasstransfer.2017.05.025.